## General Disclaimer

## One or more of the Following Statements may affect this Document

- This document has been reproduced from the best copy furnished by the organizational source. It is being released in the interest of making available as much information as possible.

- This document may contain data, which exceeds the sheet parameters. It was furnished in this condition by the organizational source and is the best copy available.

- This document may contain tone-on-tone or color graphs, charts and/or pictures, which have been reproduced in black and white.

- This document is paginated as submitted by the original source.

- Portions of this document are not fully legible due to the historical nature of some of the material. However, it is the best reproduction available from the original submission.

Produced by the NASA Center for Aerospace Information (CASI)

GCA-TR-76-1-N

CR 137832

# AIRBORNE PHOTOGRAPHY OF CHEMICAL RELEASES AND ANALYSIS OF TWILIGHT SKY BRIGHTNESS DATA

Prepared by
John F. Bedinger
Eustratios Constantinides

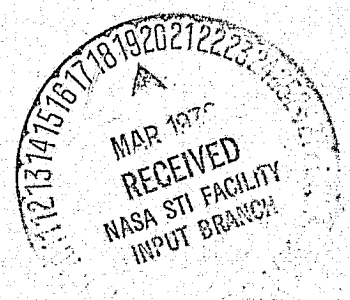


Prepared For
NATIONAL AERONAUTICS AND SPACE ADMINISTRATION
Ames Research Center
Moffett Field, California

FINAL REPORT
PHASES II AND III
CONTRACT NO. NAS2-7998

January 1976

(NASA-CR-137832) AIRBORNE PHOTOGRAPHY OF CHEMICAL RELEASES AND ANALYSIS OF TWILIGHT SKY BRIGHTNESS DATA, PHASES 1 AND 2 Final Report (GCA Corp.) 42 p HC $4.00 CSCL 04A
N76-18723
Unclas
G3/46 20808

GCA/TECHNOLOGY DIVISION
BEDFORD, MASSACHUSETTS 01730

CONTENTS

## LIST OF FIGURES

LIST OF TABLES

## INTRODUCTION PHASE II

Project Aladdin consisted of a series of 52 sounding rockets fired from Wallops Island, coinciding with the passage of the Atmospheric Explorer satellite, and coordinated with numerous ground based observations. The original rocket program included nine chemical releases for the measurement of upper-atmospheric winds which were scheduled at 3 hour intervals over a 27 hour period. The standard method of observing these releases utilizing ground sites is subject to weather restrictions which may cause costly delays or interruption of the launch sequence. A delay in the firing schedule was particularly undesirable for the Aladdin program because the Atmospheric Explorer satellite was in a favorable orbit for a limited time. The recently developed technique in which the required observations are obtained from a single high flying aircraft circumvent the weather restrictions and also allow photography of a lithium release during the daytime. The purpose of this phase of the contract was the photography of the chemical releases from aboard the Lear Jet aircraft which is owned and operated by the Airborne Science Office, NASA Ames Research Center.

The Aladdin program required the photography of chemical releases during the day, during twilight and during the night. The brightness of the releases as well as the sky brightness varies greatly for these conditions and thus different techniques and equipment are required for the useful photography of the releases. Careful layout and installation was required in order to accomodate the equipment within the limited capacity of the Lear Jet. The purpose of the various equipment and the method of installation are discussed in the next section.

## EQUIPMENT INSTALLATION

During the past three years, the methods of photographing chemical releases from an aircraft and the associated analytical procedures to obtain winds have been developed. These methods were described in the reports under contracts NASW-2308 and NASW-2450.

Photographic observation of a chemical release from an aircraft differs from that from ground sites because of (1) the changing position of the aircraft, (2) the changing orientation, (3) the limitation of exposure time due to aircraft motion, (4) more stringent requirements for pointing accuracy due to varying plane position, and (5) the necessity to continually measure, record, and correlate these parameters. Methods for obtaining and recording these data have been previously developed for the large CV990 aircraft. The use of the smaller Lear Jet required a considerably more efficient use of the available space and a reduced number of cameras and operators. The instrumentation of the aircraft was accomplished by the experienced personnel at NASA Ames Research Center. The major installations and their functions are briefly described in the following paragraphs.

It is required that the aircraft follow a precise flight path and that its position and orientation be recorded continually. Previously this information has been obtained with an Inertial Navigation System (INS) aboard the CV990 aircraft. A similar system was installed in the Lear Jet for the first time and accurate flight paths and aircraft orientation were executed and recorded. Aircraft position was determined by a ground based tracking radar with the aid of an airborne S-band transponder.

The data from the INS, the output of a time code generator, and indicators of photographic exposures were recorded on an eight channel magnetic tape recorder. Some of these data were also recorded on video tape from a display of digital voltmeters.

A major installation was a gyrostabilized mirror system with its associated controls and power suppliers. This system was used to extend the useful exposure time for the relatively dim nighttime chemical releases. This stabilized mirror system maintained the pointing angle during the exposure by correcting for aircraft motion. The system was not activated and the mirror was locked into a fixed position for the twilight and daytime releases.

The cameras are those which were installed in the CV900 previously. The twilight and daytime trails employed standard 70 mm automatic cameras with 80 mm, f 2.8 lenses which provide a useful field angle of approximately $40^{o}$. Narrowband filters and locating fiducial marks which allowed the utilization of previous star calibrations were employed during the daytime. The less bright night releases were photographed with f 1.5 lenses and employed the stabilized morror system to allow useful exposures of up to several seconds. These cameras, as well as the video camera and recorder were operated from 60 cycle power supplied by special converters installed for that purpose.

In addition to the 70 mm camera, two small television cameras and two small monitors were installed. One of these cameras was used to record data as previously indicated. The other television camera was directed toward the chemical releases as were the film cameras. The output of both of the television cameras could be received on the monitors, one of which was installed in the cabin and the other in the cockpit. The primary purpose of viewing the release was to aid in pointing of the aircraft.

Some of the equipment which was installed in the Lear Jet is shown in Figure 1. The stabilized mirror system appears on the left in Figure 1a, adjacent to two 70 mm cameras which viewed the trail through the forward window via the mirror. The video tape recorder is to the right of the camera. In Figure 1b, two other 70 mm cameras are shown in a locked position for take-off and landing. These cameras were moved forward along a guide rail into position in front of the rear window during observations. One of the television monitors and a spare 70 mm camera are shown in the foreground. The INS, power supplier, tape recorder, and various monitors which were mounted in the rear of the cabin are not shown.

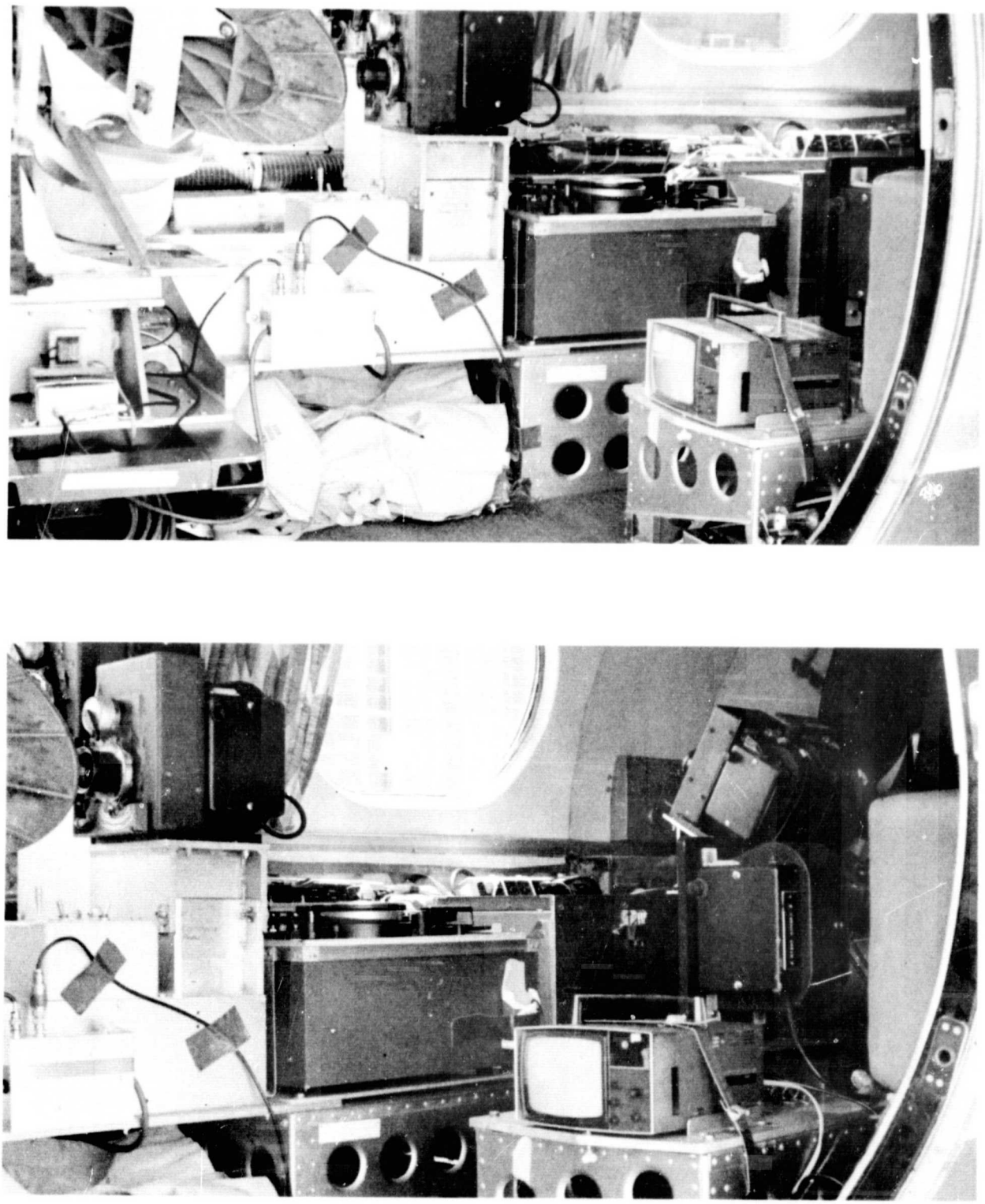

Figure 1. Equipment installation in the Lear Jet for the chemical release observations

## CHEMICAL RELEASE OBSERVATIONS

The sounding rocket firings associated with project Aladdin were originally scheduled to begin about noon on 17 June and to continue into the afternoon in the following day. Unfavorable weather conditions caused a delay until 29 June with some modification of the number and schedule of rocket firings. The delay allowed time for several test flights with the Lear Jet which were very beneficial for testing and practicing with the hastily installed equipment. The closely spaced chemical releases around twilight required equipment changes in flight and special star calibrations. Practice in those procedures was especially beneficial. Methods were developed also to cope with such problems as window fog and spurious reflection. The aircraft functioned efficiently throughout the period and difficulties which developed in the INS were corrected effectively by the highly competent personnel from Ames Research Center.

The first chemical release occurred during the evening twilight of 28 June. When a trail of sodium and lithium vapor was deposited for the purpose of testing and adjustment of the observing equipment both on the ground and in the aircraft. Good data were obtained from the Lear Jet, but widespread clouds prevented complete observations from the ground. The photographs from on board the aircraft indicated that the chemical vaporizer operated for a shorter period than expected and vapor was not deposited over the desired height range. The trail was released from the descending rocket and thus the vapor did not extend to the lower part of the region of interest; i.e., below 120 km. The release of the final trail in the Aladdin series was changed to the ascending portion of the trajectory in order to circumvent the reoccurrence of that situation.

The sequential series of chemical releases began during evening twilight on 29 June when a descending rocket ejected a puff of barium vapor followed by a series of puffs of TMA and finally a TMA trail. All ground optical sites were reported to be clear and the release was visually observed from them and from the aircraft while flying the planned path. Another release was scheduled for 20 minutes later but did not occur due to a rocket malfunction. The next scheduled release at about midnight failed also due to improper payload performance.

The second successful release occurred about 0200 on 30 June when a downtrail release of TMA was clearly observed from ground sites. The aircraft did not attempt to observe that release in order to enhance probability of more complete coverage of latter releases. The decision to not observe that release from the aircraft was precipitated by deteriorating weather conditions for the ground observations. Fog was becoming dense at Wallops Station abound midnight and in order to prevent the possibility of not being able to operate the jet from there at a later time, it was decided to move the aircraft and crew to Langley Research Center where better equipment

allows less stringent operating conditions. The ground sites were reported to be operational, so the observations from the aircraft were not considered to be essential for that release. The Lear Jet landed at Langley after the midnight flight and operated from there unitl it landed back at Wallops Station around 9 o'clock the next morning.

During that period two observation flights were made. The first lasted for about 2 1/2 hours and two releases were observed. A downtrail of TMA was successfully ejected and observed at 0330 and was followed by another TMA release at 0435 which attained only partial success due to payload difficulties. The second flight from Langley was for observation of the first daytime release of the series which was a trail of lithium vapor released at about 0855, after which the Lear landed at Wallops Station. The final flight in the series was made from Wallops and successfully observed another lithium trail at about 1320 EDT.

The releases observed from the Lear Jet are summarized in Table 1. Example photographs of the various releases are shown in Figures 2, 3, and 4.

Table 1

CHEMICAL RELEASES OBSERVED FROM THE LEAR JET

| Vehicle No. | | Released material | Launch time EDT. |
|---|---|---|---|
| AFCRL | NASA W.I. | | |
| UT9-301.1 | D2-7290 | Ba, TMA | 2106 |
| UT9-301.4 | D2-7294 | TMA | 0330 |
| PT10-301.6 | D2-7291 | Ba, TMA | 0435 |
| UT9-105.6 | D2-7296 | Na, Li | 0855 |
| UT9-301.7 | D2-7297 | Na, Li | 1320 |

Figure 2 is the evening twilight release of TMA (2106 EDT) on the downward portion of the rocket trajectory which included a series of puffs followed by a short trail. Figure 3 is another downtrail of TMA released during the nighttime (0330 EDT). Figure 4 is an uptrail release of lithium vapor released during the day (0855 EDT).

Figure 2. Downtrail release of TMA during evening twilight



ORIGINAL PAGE IS
OF POOR QUALITY

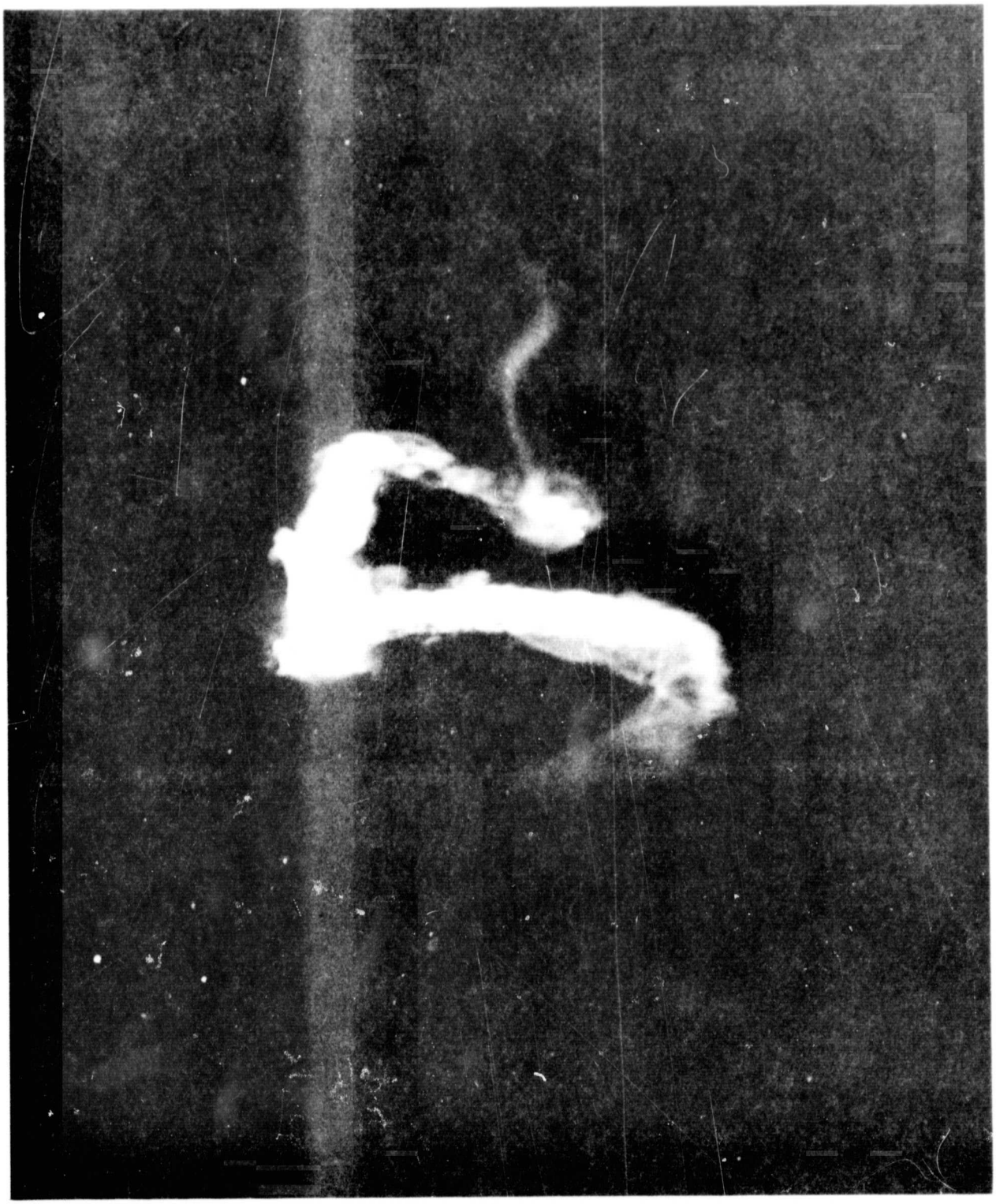

Figure 3. Downtrail release of TMA during the night



ORIGINAL PAGE IS
OF POOR QUALITY

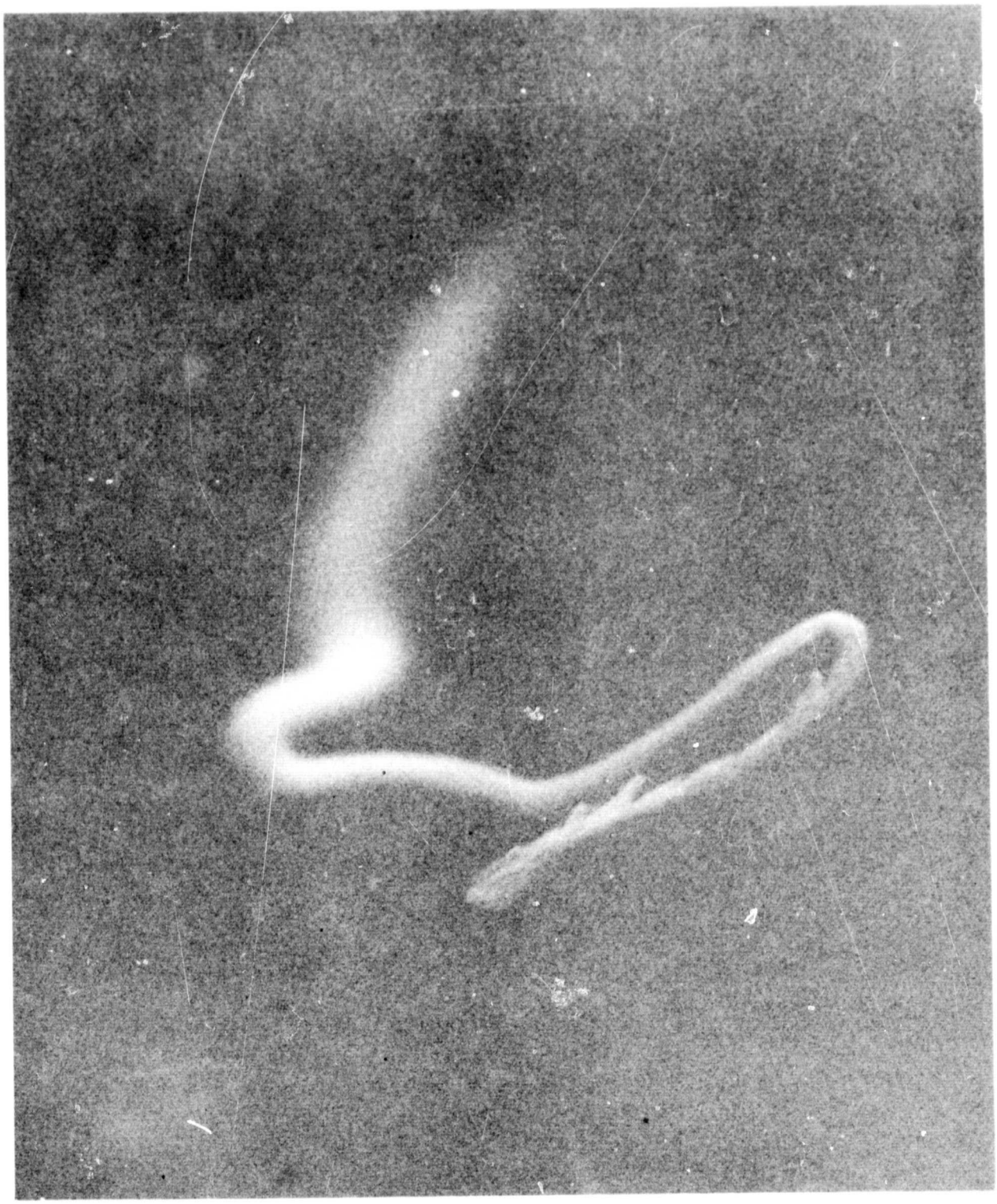

Figure 4. Uptrail release of lithium during the day



ORIGINAL PAGE IS
OF POOR QUALITY

## DATA SUMMARY

The data consist of photographs of the releases and various auxillary information which is required for the reduction process.

### Photographs of the Releases

All of the chemical releases were photographed on 70 mm Kodak 2475 film with 83 mm focal length lenses. The exposures used for the various releases are given in Table 2.

### Auxillary Information

The auxillary data were recorded in several different ways as described in Section II. The data for each flight are summarized in Tables 3 through 8. The times of the exposures are given in Local Daylight Time which is GMT minus 4 hours. The altitude of the aircraft was 40,000 ft for all observations. The north latitude and west longitude of the aircraft are given in degrees for the beginning of each exposure. Aircraft heading is in degrees True, pitch is in degrees with plus denoting nose up; roll is in degrees with plus denoting right wing down and minus denoting left wing down.

### Star Calibration

Star images for position calibration of the photographs were obtained during three of the Lear flights. Constellations which appear on frames listed in Tables 1, 2 and 3 have been identified as follows:

Table 1. Ursa Minor, Cepheus, Draco, and Cygnus.

Table 2. Ursa Minor, Cepheus, and Cassiopeia.

Table 3. Andromeda, Triangulum, and Perseus.

### Rocket Trajectory

Tabulations of the reduced radar tracking data were furnished to AFCRL by NASA, Wallops Flight Center for each of the rockets involved with the chemical releases.

Table 2

PHOTOGRAPHIC EXPOSURES FOR CHEMICAL RELEASES DURING PROJECT ALADDIN

| Rocket no. | | Time | Camera #1 | | Camera #2 | | Camera #3 | | Camera #4 | |
|---|---|---|---|---|---|---|---|---|---|---|
| AFCRL | NASA | | Stop | Exp. | Stop | Exp. | Stop | Exp. | Stop | Exp. |
| A0-7-105.7 | D2-7285 | 6/28/74 2110 LDT | 2.8 | 1/2 sec. | 2.8 | 1 sec. | 1.5 | 5 sec. | 2.8 | 1 sec. |
| UT9-301.1 | D2-7290 | 6/29/74 2106 LDT | 2.8 | 1/2 sec. | 2.8 | 1 sec. | 1.5 | 5 sec. | 2.8 | 1 sec. |
| UT9-301.4* | D2-7294 | 6/30/74 0330 LDT | 1.5 | 5 sec. | 1.5 | 5 sec. | 1.5 | 1/2; 1 sec. | 2.8 | 5 sec. |
| PT10-301.6 | D2-7291 | 6/30/74 0435 LDT | 2.8 | 1/2 sec. | 2.8 | 1 sec. | 2.8 | 5 sec. | 2.8 | 1 sec. |
| UT9-105.6+ | D2-7296 | 0855 LDT | 4 | 1/10 sec. | 4 | 1/10 sec. | 5.6 | 1/10 sec. | 4 | 1/10 sec. |
| UT9-301.7+ | D2-7297 | 1320 LDT | 4 | 1/10 sec. | 4 | 1/10 sec. | 5.6 | 1/10 sec. | 4 | 1/10 sec. |

*Camera 1 & 2 utilized stabilized mirror system.

+All cameras were equipped with narrow band filters.

Table 3

LEAR JET DATA - NASA NO. D2-7285, AFCRL NO. AO-7-105.7, LAUNCH 2110 LDT, 6/28/74

| Frame no. | Time LDT hr. | min. | sec. | Lat. deg. | Long. deg. | Heading deg. T | Pitch deg. | Roll deg. |
|---|---|---|---|---|---|---|---|---|
| 1 | 21 | 15 | 02.1 | 35.4165 | 75.0365 | 291.32 | +2.78 | +7.47 |
| 5 | 21 | 15 | 26.0 | 35.4453 | 75.0871 | 297.05 | +2.95 | +0.23 |
| 10 | 21 | 15 | 56.0 | 35.4788 | 75.1527 | 288.15 | +2.66 | +0.26 |
| 15 | 21 | 16 | 26.0 | 35.5086 | 75.2172 | 286.82 | +2.71 | +0.83 |
| 20 | 21 | 16 | 56.1 | 35.5388 | 75.2818 | 289.05 | +2.69 | +2.05 |
| 25 | 21 | 17 | 26.1 | 35.5710 | 75.3452 | 290.76 | +2.71 | +0.28 |
| 30 | 21 | 17 | 56.1 | 35.6037 | 75.4093 | 291.57 | +2.77 | -0.91 |
| 35 | 21 | 18 | 26.1 | 35.6067 | 75.4720 | 290.70 | +2.84 | -1.00 |
| 40 | 21 | 18 | 56.1 | 35.6674 | 75.5323 | 289.66 | +2.75 | -0.49 |
| 45 | 21 | 19 | 26.2 | 35.6992 | 75.5993 | 289.99 | +2.57 | -0.89 |
| 50 | 21 | 19 | 56.2 | 35.7306 | 75.6648 | 289.63 | +2.77 | +0.34 |
| 55 | 21 | 20 | 26.2 | 35.7628 | 75.7308 | 291.28 | +2.69 | +0.62 |
| 60 | 21 | 20 | 56.3 | 35.7959 | 75.7979 | 291.48 | +2.37 | -0.02 |
| 65 | 21 | 21 | 26.3 | 35.8295 | 75.8647 | 292.48 | +2.48 | +0.66 |
| 70 | 21 | 21 | 56.3 | 35.8650 | 75.9302 | 296.87 | +2.37 | +2.95 |
| 75 | 21 | 22 | 26.4 | 35.9053 | 75.9938 | 301.60 | +2.26 | +5.07 |
| 80 | 21 | 22 | 56.4 | 35.9523 | 76.0549 | 308.33 | +2.30 | +3.86 |
| 85 | 21 | 23 | 26.4 | 36.0038 | 76.1092 | 313.36 | +2.35 | +1.12 |
| 90 | 21 | 23 | 56.4 | 36.0568 | 76.1583 | 311.64 | +2.53 | -1.84 |
| 95 | 21 | 24 | 26.4 | 36.1032 | 76.2184 | 300.94 | +2.11 | +7.23 |
| 100 | 21 | 24 | 56.4 | 36.1513 | 76.2752 | 311.10 | +2.40 | -10.81 |

Table 4

LEAR JET DATA - NASA NO. D2-7290, AFCRL NO. UT9-301.1,
LAUNCH 2106 LDT, 6/29/74

| Frame no. | Time LDT hr. | min. | sec. | Lat. deg. | Long. deg. | Heading deg. T | Pitch deg. | Roll deg. |
|---|---|---|---|---|---|---|---|---|
| 1 | 21 | 08 | 56 | 35.4722 | 74.7993 | 259.51 | +2.75 | -0.39 |
| 5 | 21 | 09 | 20 | 35.4713 | 74.8495 | 264.39 | +2.82 | +2.20 |
| 10 | 21 | 09 | 50 | 35.4761 | 74.9132 | 269.24 | +2.32 | +4.02 |
| 15 | 21 | 10 | 20 | 35.4854 | 74.9780 | 274.10 | +2.30 | -0.20 |
| 20 | 21 | 10 | 50 | 35.4956 | 75.0414 | 272.48 | +2.40 | -0.94 |
| 25 | 21 | 11 | 20 | 35.5051 | 75.1071 | 274.10 | +2.36 | +3.77 |
| 30 | 21 | 11 | 50 | 35.5179 | 75.1722 | 275.72 | +2.46 | -2.73 |
| 35 | 21 | 12 | 20 | 35.5294 | 75.2386 | 277.34 | +2.45 | +2.07 |
| 40 | 21 | 12 | 50 | 35.5431 | 75.3035 | 275.72 | +1.95 | +2.64 |
| 45 | 21 | 13 | 20 | 35.5606 | 75.3674 | 282.04 | +2.36 | +5.38 |
| 50 | 21 | 13 | 50 | 35.5852 | 75.4305 | 287.08 | +2.50 | +3.05 |
| 55 | 21 | 14 | 20 | 35.6146 | 75.4919 | 290.16 | +2.48 | -0.13 |
| 60 | 21 | 14 | 50 | 35.6446 | 75.5484 | 291.79 | +2.34 | +0.86 |
| 65 | 21 | 15 | 20.1 | 35.6769 | 75.6088 | 293.56 | +2.38 | +3.82 |
| 70 | 21 | 15 | 50.1 | 35.7135 | 75.6666 | 289.29 | +2.39 | +2.73 |
| 75 | 21 | 16 | 20.2 | 35.7534 | 75.7198 | 301.58 | +2.45 | -8.75 |
| 80 | 21 | 16 | 50.2 | 35.7915 | 75.7739 | 301.58 | +2.29 | +2.77 |
| 85 | 21 | 17 | 20.2 | 35.8323 | 75.8294 | 301.67 | +2.57 | -0.44 |
| 90 | 21 | 17 | 50.2 | 35.8719 | 75.8837 | 296.80 | +2.52 | -3.87 |
| 95 | 21 | 18 | 20.2 | 35.9067 | 75.9415 | 296.85 | +2.38 | -3.06 |
| 100 | 21 | 18 | 50.2 | 35.9375 | 76.0004 | 291.79 | +2.36 | -0.92 |
| 105 | 21 | 19 | 20.3 | 35.9667 | 76.0642 | 291.80 | +2.32 | -0.31 |
| 110 | 21 | 19 | 50.2 | 35.9931 | 76.1258 | 290.16 | +2.39 | -0.66 |

Table 5

LEAR JET DATA - NASA NO. D2-7294, AFCRL NO. UT9-301.4,
LAUNCH 0330 LDT, 6/30/74

| Frame no. | Time LDT hr. | min. | sec. | Lat. deg. | Long. deg. | Heading deg. T | Pitch deg. | Roll deg. |
|---|---|---|---|---|---|---|---|---|
| 1 | 03 | 33 | 00.2 | 35.4168 | 74.6964 | 256.03 | +2.68 | -0.39 |
| 5 | 03 | 33 | 23 | 35.4145 | 74.7402 | 259.29 | +2.52 | +0.32 |
| 10 | 03 | 33 | 53 | 35.4266 | 74.8019 | 280.42 | +3.09 | +3.20 |
| 15 | 03 | 34 | 23 | 35.4611 | 74.8550 | 298.29 | +2.63 | +2.66 |
| 20 | 03 | 34 | 53 | 35.5027 | 74.9028 | 298.30 | +2.57 | +0.57 |
| 25 | 03 | 35 | 23 | 35.5449 | 74.9506 | 298.30 | +2.39 | -0.61 |
| 30 | 03 | 35 | 53 | 35.5885 | 74.9981 | 296.85 | +2.38 | +4.18 |
| 35 | 03 | 36 | 23 | 35.6364 | 75.0403 | 304.79 | +2.29 | +3.55 |
| 40 | 03 | 36 | 53 | 35.6879 | 75.0775 | 301.58 | +2.18 | -0.94 |
| 45 | 03 | 37 | 23 | 35.7408 | 75.1139 | 296.85 | +2.23 | -1.00 |
| 50 | 03 | 37 | 53 | 35.7932 | 75.1506 | 290.16 | +2.18 | -0.18 |
| 55 | 03 | 38 | 23 | 35.8454 | 75.1876 | 285.30 | +2.36 | -0.62 |
| 60 | 03 | 38 | 53.1 | 35.8998 | 75.2223 | 278.78 | +2.21 | -2.62 |
| 65 | 03 | 39 | 23.1 | 35.9540 | 75.2533 | 278.80 | +2.23 | -3.87 |
| 70 | 03 | 39 | 53.1 | 36.0123 | 75.2762 | 278.80 | +2.36 | -5.95 |
| 75 | 03 | 40 | 23.1 | 36.0739 | 75.2897 | 262.53 | +2.45 | -4.77 |
| 80 | 03 | 40 | 53.1 | 36.1368 | 75.2976 | 278.80 | +2.39 | -1.16 |
| 85 | 03 | 41 | 23.1 | 36.2001 | 75.3017 | 278.80 | +2.57 | -5.19 |
| 90 | 03 | 41 | 53.1 | 36.2641 | 75.3003 | 262.53 | +2.59 | -0.92 |
| 95 | 03 | 42 | 23.1 | 36.3283 | 75.2960 | 278.80 | +2.55 | -2.44 |

Table 6

LEAR JET DATA - NASA NO. D2-7295, AFCRL NO. PT10-301.6,
LAUNCH 0435 LDT, 6/30/74

| Frame no. | Time LDT hr. | min.. | sec. | Lat. deg. | Long. deg. | Heading deg. T | Pitch deg. | Roll deg. |
|---|---|---|---|---|---|---|---|---|
| 1 | 04 | 39 | 20 | 35.5543 | 75.0822 | not recorded | +3.66 | +0.13 |
| 5 | 04 | 39 | 44 | 35.5728 | 75.1194 | | +3.77 | -0.30 |
| 10 | 04 | 40 | 14 | 35.5962 | 75.1660 | | +4.04 | +2.02 |
| 15 | 04 | 40 | 44 | 35.6247 | 75.2125 | | +4.20 | -5.93 |
| 20 | 04 | 41 | 14 | | | | +4.59 | -0.88 |
| 25 | 04 | 41 | 44 | no data | | | +4.36 | +7.88 |
| 30 | 04 | 42 | 14 | | | | +4.38 | +3.38 |
| 35 | 04 | 42 | 44 | 35.7671 | 75.3340 | | +4.52 | +0.59 |
| 40 | 04 | 43 | 14 | 35.8127 | 75.3522 | | +4.30 | -1.05 |
| 45 | 04 | 43 | 44 | 35.8586 | 75.3725 | | +4.18 | -0.96 |
| 50 | 04 | 44 | 14 | 35.9053 | 75.3924 | | +3.82 | +2.82 |
| 55 | 04 | 44 | 44 | 35.9542 | 75.4081 | | +3.61 | +2.05 |
| 60 | 04 | 45 | 14 | 36.0056 | 75.4195 | | +3.54 | +1.63 |
| 65 | 04 | 45 | 44 | 36.0574 | 75.4313 | | +3.48 | -2.86 |
| 70 | 04 | 46 | 14 | 36.1081 | 75.4483 | | +3.18 | -3.29 |
| 75 | 04 | 46 | 44 | 36.1528 | 75.4787 | | +3.04 | +5.29 |
| 80 | 04 | 47 | 14 | 36.2034 | 75.4969 | | +3.30 | -1.05 |
| 85 | 04 | 47 | 44 | 36.2554 | 75.5137 | | +3.30 | +1.89 |
| 90 | 04 | 48 | 14 | 36.3092 | 75.5274 | | +3.00 | +1.71 |
| 95 | 04 | 48 | 44 | 36.3642 | 75.5382 | | +2.96 | +0.96 |

Table 7

LEAR JET DATA - NASA NO. D2-7296; AFCRL NO. UT9-105.9,
LAUNCH 0855 LDT, 6/30/74

| Frame no. | Time LDT hr. | min. | sec. | Lat. deg. | Long. deg. | Heading deg. T | Pitch deg. | Roll deg. |
|---|---|---|---|---|---|---|---|---|
| 1 | 08 | 56 | 01.4 | 38.9386 | 74.5527 | 110.17 | +3.50 | +1.66 |
| 5 | 08 | 56 | 25.4 | 38.9242 | 74.4940 | 110.17 | +2.89 | +0.23 |
| 10 | 08 | 56 | 55.4 | 38.9047 | 74.4199 | 114.89 | +3.25 | +4.21 |
| 15 | 08 | 57 | 25.4 | 38.8831 | 74.3477 | 116.29 | +3.16 | +0.11 |
| 20 | 08 | 57 | 55.4 | 38.8603 | 74.2755 | 117.91 | +3.25 | +2.43 |
| 25 | 08 | 58 | 25.4 | 38.8351 | 74.2045 | 117.91 | +3.07 | +3.79 |
| 30 | 08 | 58 | 55.4 | 38.8056 | 74.1363 | 128.53 | +3.24 | +2.84 |
| 35 | 08 | 59 | 25.4 | 38.7722 | 74.0715 | 130.15 | +3.31 | +0.70 |
| 40 | 08 | 59 | 55.4 | 38.7380 | 74.0018 | 130.15 | +3.07 | -3.03 |
| 45 | 09 | 00 | 25.4 | 38.7046 | 73.9426 | 130.15 | +2.77 | +4.25 |
| 50 | 09 | 00 | 55.5 | 38.6683 | 73.8804 | 120.97 | +2.68 | +1.09 |
| 55 | 09 | 01 | 25.6 | 38.6294 | 73.8221 | 139.33 | +3.33 | +4.45 |
| 60 | 09 | 01 | 55.7 | 38.5855 | 73.7681 | 148.50 | +3.04 | +1.66 |
| 65 | 09 | 02 | 25.7 | 38.5396 | 73.7185 | 146.89 | +2.96 | +0.00 |
| 70 | 09 | 02 | 55.7 | 38.4940 | 73.6693 | 148.51 | +2.75 | +0.02 |
| 75 | 09 | 03 | 25.8 | 38.4467 | 73.6213 | 149.95 | +2.98 | +1.80 |
| 80 | 09 | 03 | 55.8 | 38.3979 | 73.5762 | 153.02 | +3.11 | +0.00 |
| 85 | 09 | 04 | 25.9 | 38.3484 | 73.5313 | 153.02 | +3.25 | +0.05 |
| 90 | 09 | 04 | 55.9 | 38.2989 | 73.4883 | 154.63 | +3.04 | +1.09 |
| 95 | 09 | 05 | 25.9 | 38.2481 | 73.4474 | 154.63 | +3.11 | +0.32 |
| 100 | 09 | 05 | 56.0 | 38.1955 | 73.4082 | 157.70 | +2.77 | +1.16 |

Table 8

LEAR JET DATA - NASA NO. D2-7297, AFCRL NO. UT9-301.7,
LAUNCH 1320 LDT, 6/30/74

| Frame no. | Time LDT hr. | min. | sec. | Lat. deg. | Long. deg. | Heading deg. T | Pitch deg. | Roll deg. |
|---|---|---|---|---|---|---|---|---|
| 1 | 13 | 21 | 00 | 35.7944 | 75.6664 | 275.49 | not recorded | +1.64 |
| 5 | 13 | 21 | 24.4 | 35.8037 | 75.7229 | 284.48 | | +4.93 |
| 10 | 13 | 21 | 54.5 | 35.8208 | 75.7921 | 288.08 | | +4.73 |
| 15 | 13 | 22 | 24.5 | 35.8431 | 75.8582 | 291.68 | | +1.73 |
| 20 | 13 | 22 | 54.8 | 35.8688 | 75.9237 | 297.07 | | +2.29 |
| 25 | 13 | 23 | 25 | 35.8974 | 75.9870 | 286.28 | | +5.91 |
| 30 | 13 | 23 | 55.2 | 35.9316 | 76.0471 | 307.86 | | +4.45 |
| 35 | 13 | 24 | 25.5 | 35.9714 | 76.1036 | 315.05 | | +1.46 |
| 40 | 13 | 24 | 55.8 | 36.0127 | 76.1574 | 316.85 | | +1.84 |
| 45 | 13 | 25 | 26 | 36.0585 | 76.2093 | 318.65 | | +1.88 |
| 50 | 13 | 25 | 56 | 36.1044 | 76.2593 | 322.24 | | +0.09 |
| 55 | 13 | 26 | 26.2 | 36.1519 | 76.3080 | 324.04 | | -2.15 |
| 60 | 13 | 26 | 56.2 | 36.1992 | 76.3560 | 324.04 | | +1.86 |
| 65 | 13 | 27 | 26.3 | 36.2478 | 76.4009 | 327.64 | | +3.30 |
| 70 | 13 | 27 | 56.5 | 36.2987 | 76.4446 | 331.23 | | +2.77 |
| 75 | 13 | 28 | 26.4 | 36.3528 | 76.4824 | 334.83 | | -1.91 |
| 80 | 13 | 28 | 56.5 | 36.4052 | 76.5229 | 329.43 | | -1.67 |
| 85 | 13 | 29 | 26.6 | 36.4562 | 76.5654 | 327.64 | | +0.38 |
| 90 | 13 | 29 | 56.6 | 36.5071 | 76.6085 | 329.43 | | +1.18 |
| 95 | 13 | 30 | 26.6 | 36.5588 | 76.6496 | 331.23 | | +1.46 |
| 100 | 13 | 30 | 56.7 | 36.6127 | 76.6880 | 333.03 | | +2.52 |

## INTRODUCTION PHASE III

Numerous photographs of the brightness of the twilight sky were obtained during the observations of the comet Kohoutek which were reported in Phase I of this contract. Densitometry and analysis of a few of these photographs indicated that the effects of absorption in the Chappius bands of ozone were indicated by a minimum in brightness, around 0.6 $\mu$. However, the extent and precision of the initial analysis was insufficient to determine accurately the magnitude of the effect or the usefulness of the results for the investigation of atmospheric ozone.

A more extensive analysis of the twilight sky photographs is reported here. The results indicate that the quality and completeness of these data severely limit the interpretation of the results. The primary purpose of the photographs was the measurement of the brightness of the comet within specified wavelength intervals and the exposure and development procedures were chosen for that purpose. These procedures were adjusted to provide maximum contrast for the unexpectedly dim comet image which was unfavorable for the sky brightness observations because only the wideband filters provided data useful for densitometry. In addition, the variability of the procedures increased the uncertainty in the comparison of the data for different camera and filter combinations.

However, the results clearly reveal effects of the absorption by ozone and thus contain information concerning the ozone distribution. The potential value of such information is discussed in Section IX of this report. The data are described in Section VI. The methods of tabulation and analysis of the data are described in Section VII and VIII.

## DESCRIPTION OF TWILIGHT SKY PHOTOGRAPHS

The photographs were obtained from onboard the NASA CV-990 aircraft at an altitude of 40,000 ft off the coast of California during January 1974. The geometry of the observations is shown in Figure 5. The observations are made from the aircraft position, A, at various elevation angles, $\Theta$, for differing solar depression angles, $\delta$. The widely varying effects of scattering and absorption of the solar rays for the integrated observing path are illustrated at selected points p.

All photographs were recorded on 70 mm roll film Kodak 2475, with 80 mm focal length lenses. Data were obtained with broad band filters, Wratten 15, 23A, and 29; narrow band interference filters centered at 5890A and 6708A; and with no filters. The transmissions of the filters are shown in Figure 6. Varying exposures required for the different filters and for changing sky brightness were obtained with adjustments of the aperture stops and length of exposure. The field of view of the cameras contained some portion of the ocean, the horizon (sometimes cloudy), and the twilight sky in the solar direction. An isophote of the entire field for a typical photograph is shown in Figure 7. The linearity of the camera system and the ability to discriminate sky brightness variations are clearly demonstrated. The data were obtained from densitometry along a line normal to the horizon and lying in a plane containing the sun and the aircraft so that displacement from the horizon along this line corresponds to a specific elevation angle. An example of a density profile is shown in Figure 8. The method of tabulation of these data is described in Section VII.

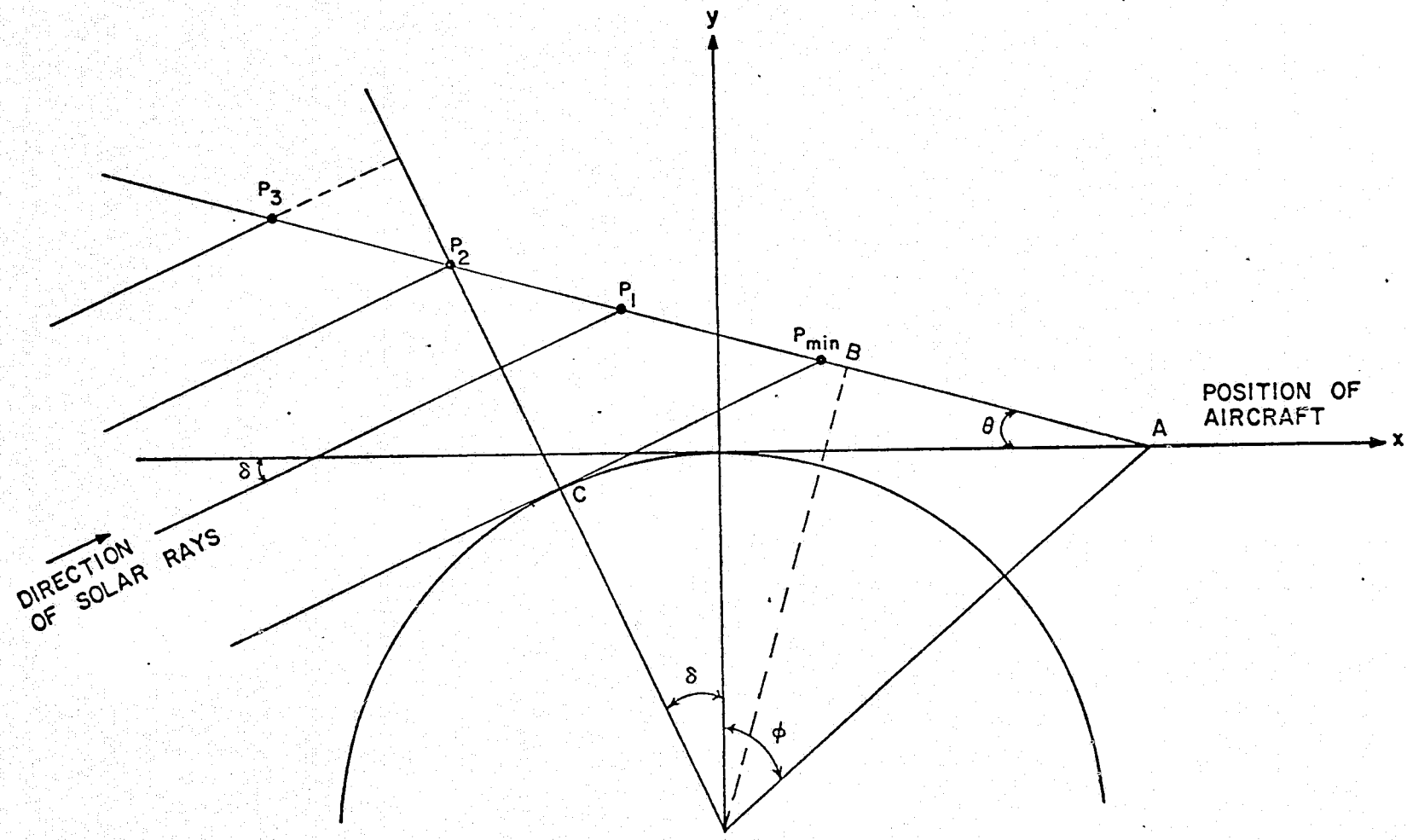


Figure 5. Geometry of the twilight sky observations

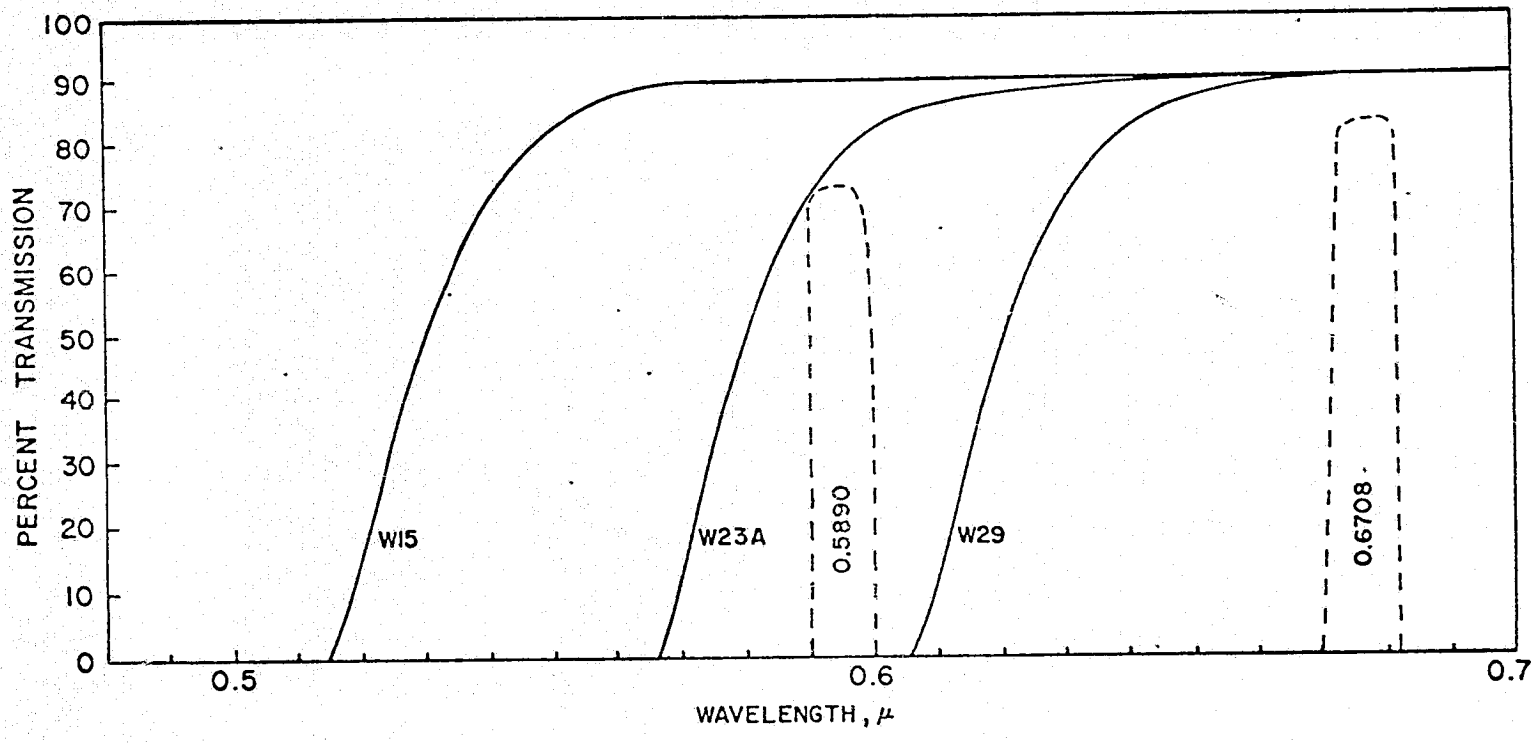


Figure 6. Transmission of filters used in sky observations

# EDP SCANNING MICROSCOPE

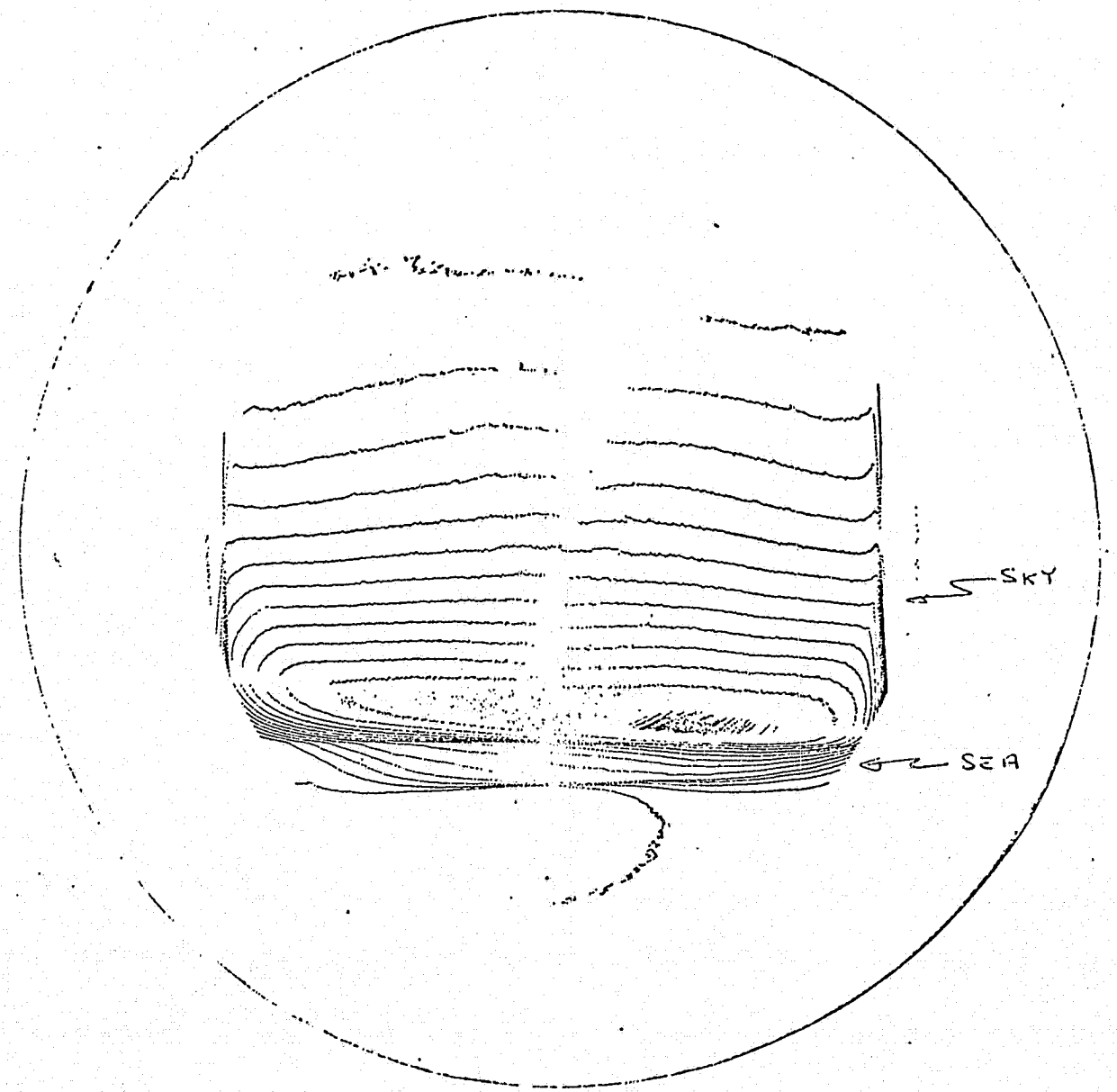


SAMPLE GCA 71 6.140
MAGNIFICATION 2
SCANNING APERTURE 30 mil
CONTOUR INTERVAL
DATE 4-26-74

PHOTOMETRICS, INC.
442 MARRETT RD., LEXINGTON, MASS. 02173
(617) 862-8050

Figure 7. Isophote of a typical sky photograph

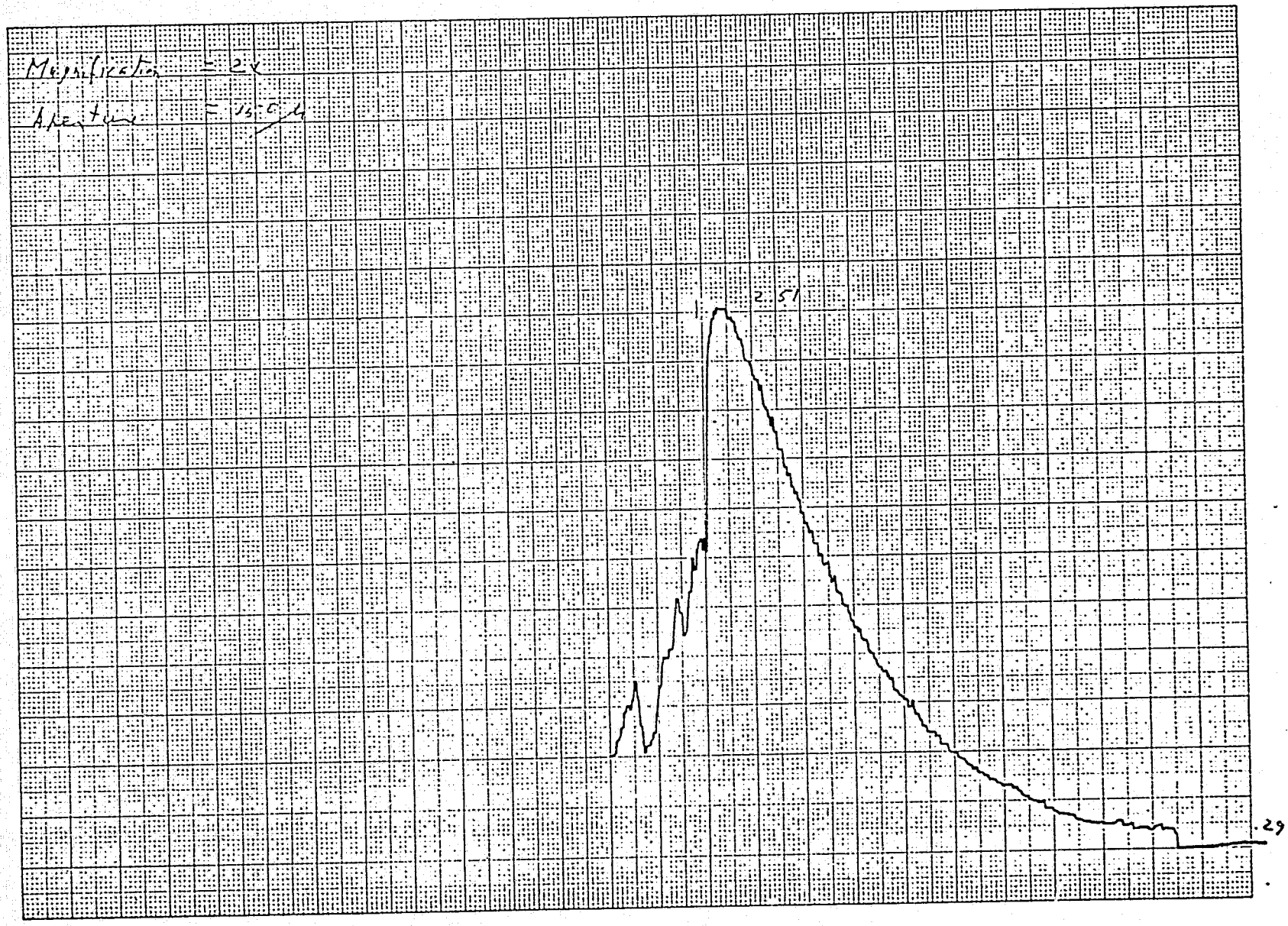


Figure 8. Density profile from a typical twilight sky photograph

## TABULATION OF TWILIGHT SKY DATA

A successive exposure sequence of 22 photographs was densitometered as described in Section VI. Relative densities of the twilight sky were generated from the horizon to 12° elevation for the interval between a solar depression angle of 1 and 6 degrees. The exposure sequence beginning with no filter was continued with Wratten filters no. 15, 23A, and 29 and ended with interference filters at 5890 and 6700A. Density values and corresponding elevation angles were tabulated at density intervals of 0.1 which produced about 20 points for each density profile. The data for each profile were then represented by a polynomial and density values were tabulated at even elevation angles from 1 to 10° and at 12°. As an example of errors associated with this process, the measured data from the third photograph in the sequence, frame number 3, is tabulated in Table 9. The elevation angle is listed in the first column, measured film density in the second, calculated density from the polynomial representation in the third and the error (difference between columns 2 and 3) in the last column. The density values at even elevation angles which were used in the analysis are give in Table 10.

Table 9

EXAMPLE OF POLYNOMIAL REPRESENTATION OF DATA

FRAME= 3

| N | ELEV | DEN | CDEN | ERROR |
|---|---|---|---|---|
| 1 | 1.720 | 2.510 | 2.533 | .023 |
| 2 | 2.924 | 2.388 | 2.368 | -.019 |
| 3 | 3.440 | 2.286 | 2.290 | .005 |
| 4 | 4.300 | 2.184 | 2.155 | -.029 |
| 5 | 4.885 | 2.082 | 2.000 | -.022 |
| 6 | 5.504 | 1.980 | 1.959 | -.021 |
| 7 | 5.917 | 1.878 | 1.892 | .014 |
| 8 | 6.536 | 1.776 | 1.792 | .016 |
| 9 | 7.086 | 1.674 | 1.705 | .031 |
| 10 | 7.774 | 1.572 | 1.599 | .028 |
| 11 | 8.531 | 1.470 | 1.488 | .018 |
| 12 | 9.460 | 1.368 | 1.360 | -.008 |
| 13 | 10.320 | 1.266 | 1.250 | -.016 |
| 14 | 11.111 | 1.164 | 1.157 | -.006 |
| 15 | 12.040 | 1.062 | 1.059 | -.003 |
| 16 | 13.347 | .960 | .939 | -.021 |
| 17 | 14.586 | .858 | .843 | -.014 |
| 18 | 15.824 | .756 | .763 | .008 |
| 19 | 17.888 | .654 | .658 | .004 |
| 20 | 19.952 | .552 | .575 | .023 |
| 21 | 23.736 | .450 | .437 | -.012 |
| 22 | 33.024 | .327 | .328 | .001 |

Table 10

DENSITIES AT EVEN ELEVATION ANGLES

FRAME= 3

| N | ELEV | DEN |
|---|---|---|
| 1 | 1.000 | 2.615 |
| 2 | 2.000 | 2.497 |
| 3 | 3.000 | 2.357 |
| 4 | 4.000 | 2.203 |
| 5 | 5.000 | 2.041 |
| 6 | 6.000 | 1.878 |
| 7 | 7.000 | 1.718 |
| 8 | 8.000 | 1.566 |
| 9 | 9.000 | 1.422 |
| 10 | 10.000 | 1.290 |
| 11 | 12.000 | 1.063 |

## DETERMINATION OF RELATIVE INTENSITY AND ATMOSPHERIC ATTENUATION

The spectral sensitivty of the film, the transmission characteristic of the filters and the exposure for each frame were used to transform the density values into relative intensities normalized to an aperture setting of f/11, and to a 0.01 second exposure time. The flux of wavelength, $\lambda$, passing through filter, N, was represented as,

$$I(\lambda,N) = S(\lambda) \cdot F(\lambda) \cdot G(\lambda,N) \cdot A(\lambda)$$

where $S(\lambda)$ is the solar flux at wavelength, $\lambda$,
$F(\lambda)$ is the film sensitivity at $\lambda$,
$G(\lambda,N)$ is the transmission at $\lambda$ for filter, N, and
$A(\lambda)$ is the atmospheric attenuation at $\lambda$.

The measured intensities for filter, N, may be represented as,

$$E(N) = \int_{\lambda\ \min}^{\lambda\ \max} d\lambda\ I(\lambda,N)$$

where $\lambda$ min and $\lambda$ max are the wavelength limits of the filtered region.

A mean wavelength for each filtered region was determined as follows.

$$\overline{\lambda^*(N)} = \int_{\lambda\ \min}^{\lambda\ \max} d\lambda \cdot \lambda \cdot I(\lambda,N) \Big/ E(N)$$

which was approximated by,

$$\overline{\lambda(N)} = \frac{\int_{\lambda\ \min}^{\lambda\ \max} d\lambda \cdot \lambda \cdot S(\lambda) \cdot F(\lambda) \cdot G(\lambda,N)}{\int_{\lambda\ \min}^{\lambda\ \max} d\lambda \cdot S(\lambda) \cdot F(\lambda) \cdot G(\lambda,N)}$$

Utilizing the filters listed in Section III, and the differences between filtered regions, a total of 12 effective average wavelengths and associated intensities were determined. These regions are listed in Table 11, together with an effective band width, $\Delta\lambda$, which was determined from

$$\Delta\lambda(N)^2 = \overline{\lambda^2(N)} - \overline{\lambda(N)}^2$$

where

$$\overline{\lambda^2(N)} = \int_{\lambda\ \min}^{\lambda\ \max} d\lambda \cdot \lambda^2 \cdot I(\lambda,N)/E(N)$$

Table 11

LIST OF FILTERED REGIONS

| Region No. | Filter name | $\overline{\lambda_\mu}$ | $\Delta\lambda_\mu$ |
|---|---|---|---|
| 1 | None | 0.490 | $\pm$ 0.108 |
| 2 | W15 | 0.610 | $\pm$ 0.047 |
| 3 | W23A | 0.635 | $\pm$ 0.033 |
| 4 | W29 | 0.655 | $\pm$ 0.021 |
| 5 | (1-2) | 0.430 | $\pm$ 0.075 |
| 6 | (1-3) | 0.448 | $\pm$ 0.083 |
| 7 | (1-4) | 0.463 | $\pm$ 0.091 |
| 8 | (2-3) | 0.559 | $\pm$ 0.023 |
| 9 | (2-4) | 0.577 | $\pm$ 0.029 |
| 10 | (3-4) | 0.601 | $\pm$ 0.016 |
| 11 | 5890 | 0.594 | $\pm$ 0.003 |
| 12 | 6708 | 0.677 | $\pm$ 0.003 |

Typical values of log E(N) for the 12 effective wavelengths are shown in Figure 9 for a constant elevation angle of 2 degrees and even solar depression angles of 1 through 6 degrees. The minimum around 0.6 $\mu$ is clearly evident. Similar data for an elevation angle of 5 degrees is shown in Figure 10. The minimum around 0.6 $\mu$ is depicted in a different manner in Figure 11 in which some of the data from Figure 10 is plotted versus solar depression angle. The minimum value, 0.589, and two values about 0.05 $\mu$ on either side of the minimum vary smoothly throughout the observing period.

The data were tabulated in a different form by defining the average atmospheric attenuation, $\overline{A(N)}$ as follows:

$$\overline{A(N)} = E(N) / \int_{\lambda\ \min}^{\lambda\ \max} d\lambda \cdot S(X) \cdot F(\lambda) \cdot G(\lambda,N)$$

Typical values from this computation appear in Figures 12 and 13 in which log $\overline{A(N)}$ is shown for varying solar depression angles. The increased attenuation around 0.6 $\mu$ is evident but the irregularities in the data are too great to allow an accurate determination of the magnitude, even after the averaging process.

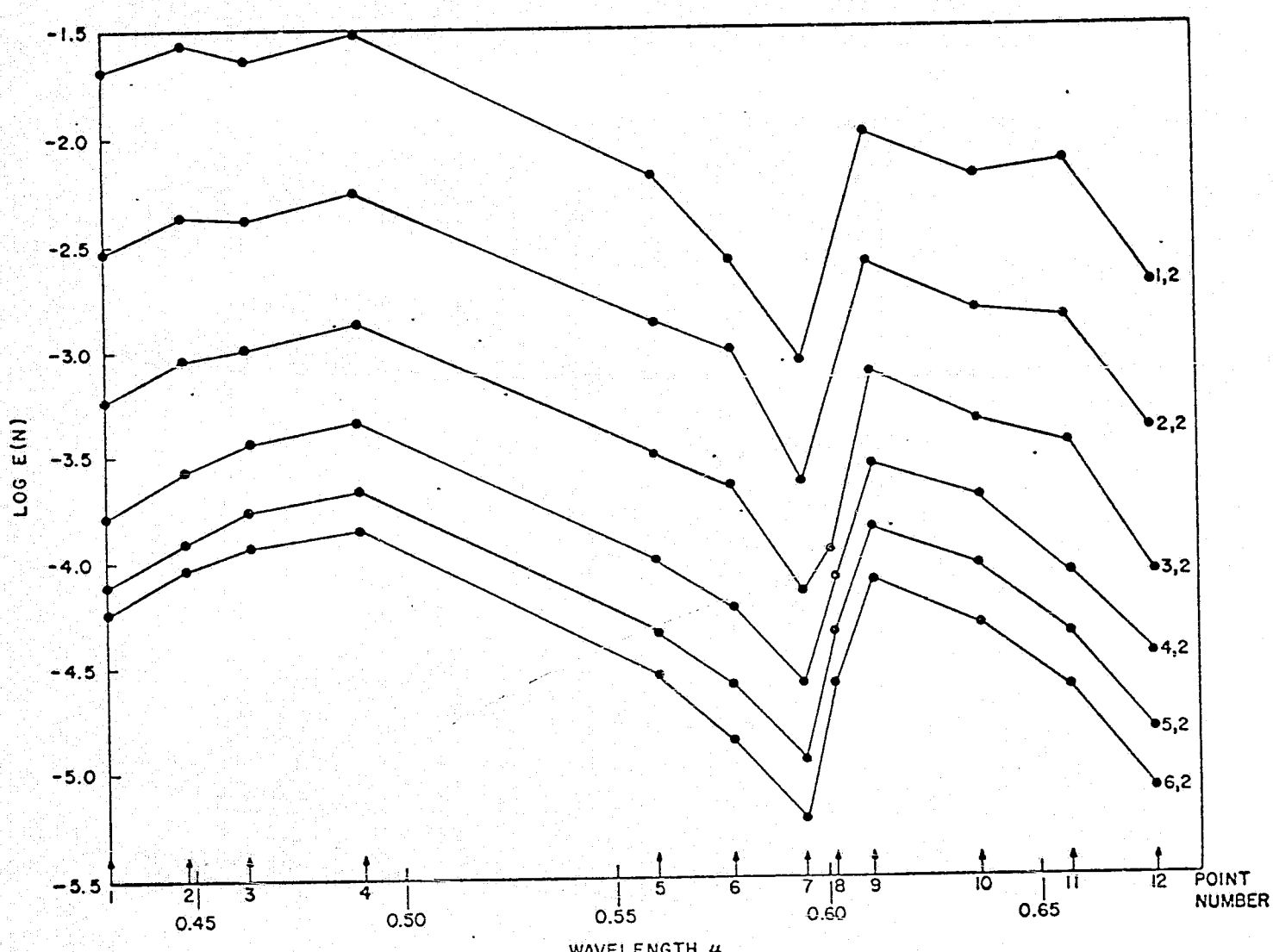


Figure 9. Log E(N) for elevation angle of 2 degrees and SDA of 1 to 6 degrees

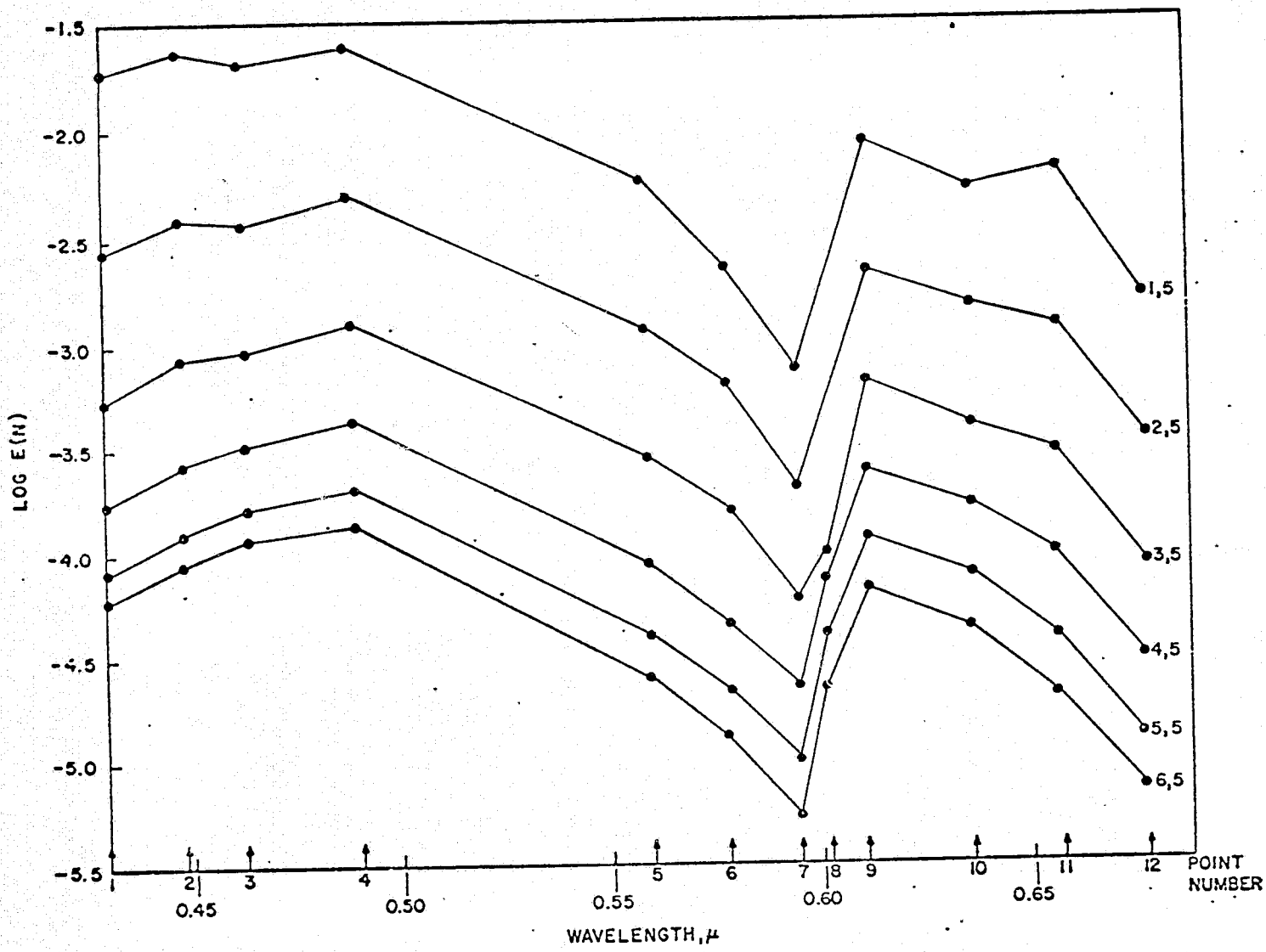


Figure 10. Log E(N) for elevation angle of 5 degrees

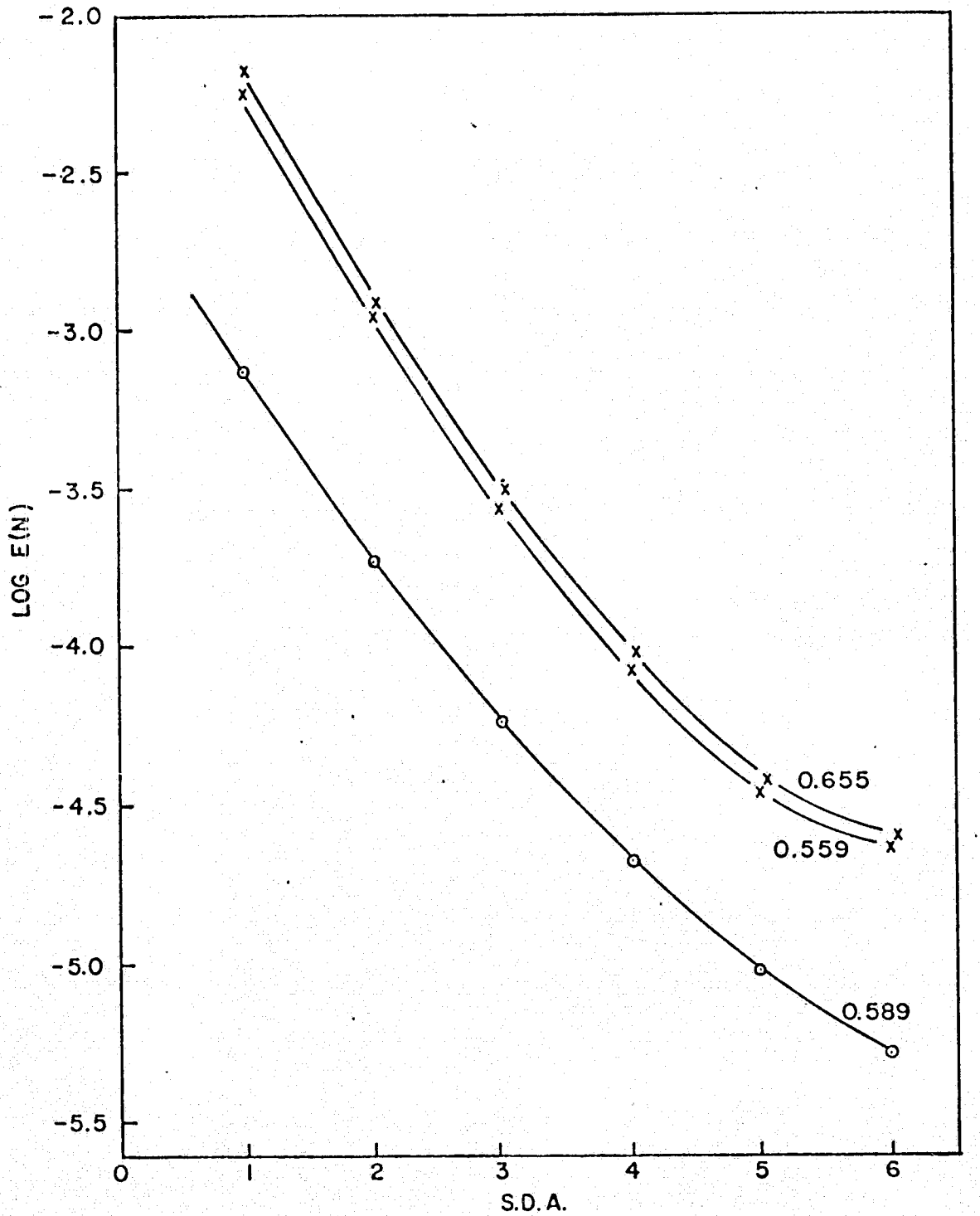


Figure 11. Log E(N) versus SDA for three wavelength intervals

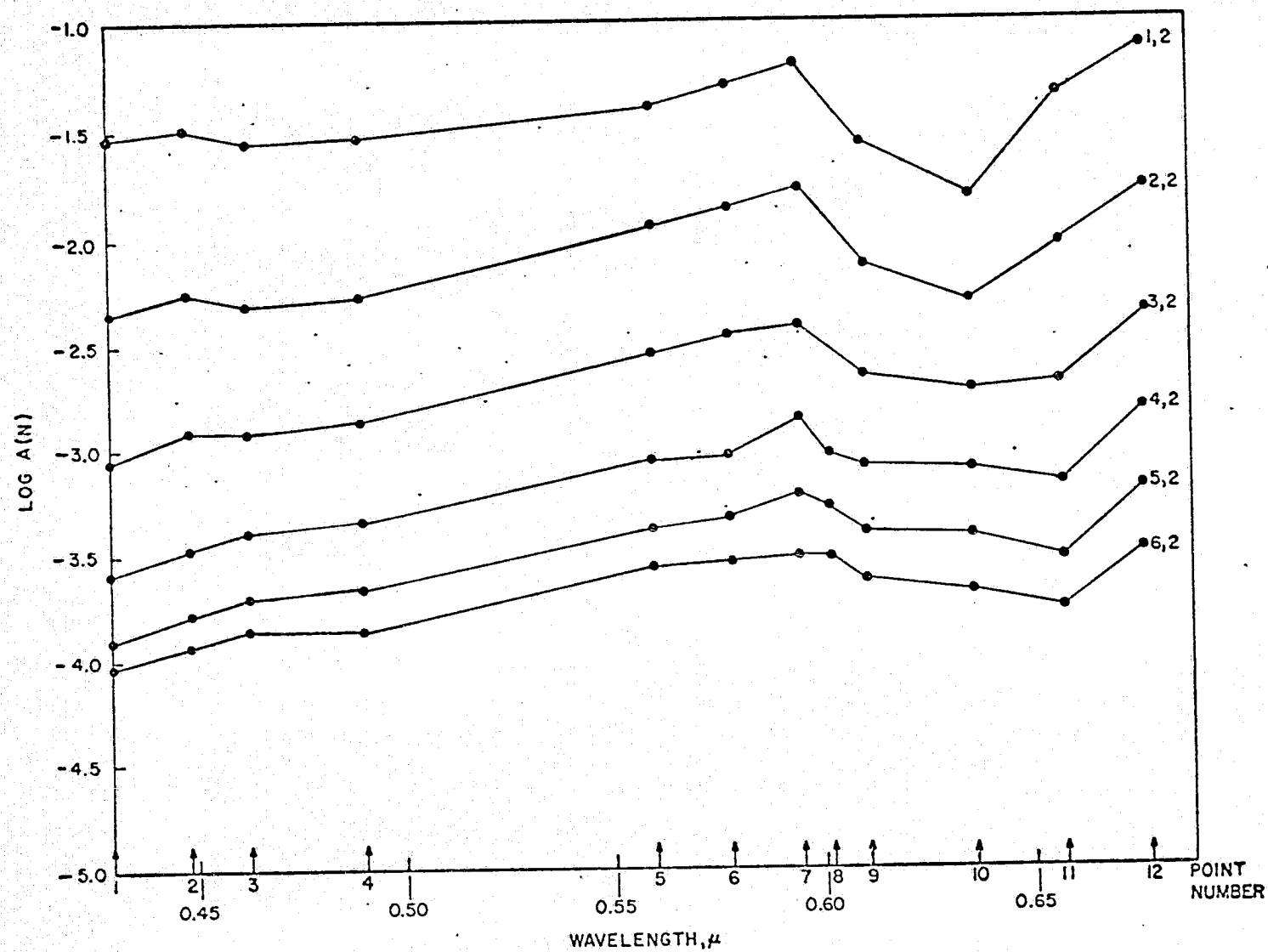


Figure 12. Log A(N) for elevation angle of 2 degrees and SDA of 1 to 6 degrees

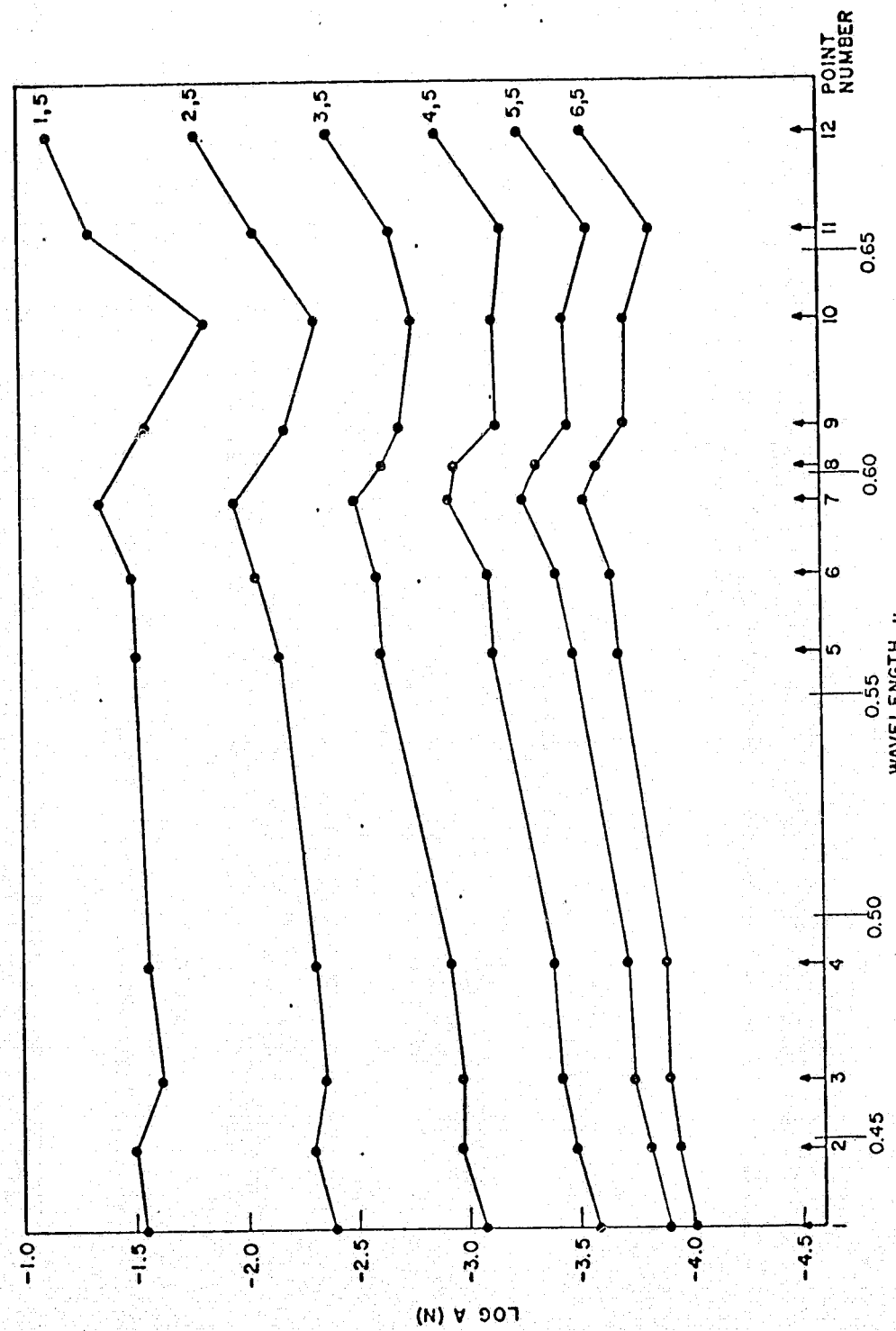


Figure 13. Log A(N) for elevation angle of 5 degrees

## DISCUSSION

The special limitations of these photographic data were stated previously. There are also general difficulties associated with calibration and processing of photographic records especially if absolute values of brightness are desired as functions of wavelength, time, and direction. However, the same type of data may be recorded with photoelectric methods which allow accurate, continuous calibration and recording of intensity and the other parameters. Thus the effectiveness of the general observational method should be determined independent of the photographic difficulties. For instance, a scanning spectrophotometer with a photoelectric sensor, could record an accurately calibrated twilight sky profile with all necessary information for direct computer processing. The uncertainties associated with these photographic data and processing would be eliminated.

The comparison of the measurements obtained from one unique sunset with the results derived from a general theoretical model allows only general conclusions at best. In this instance the difficulties are increased because the data were taken on board the aircraft and the model chosen for comparison depicts ground based measurements. The model by Adams, Plass and Kattawar (1974) was chosen because it is the most recent and includes the effects of aerosols. The effects of ozone and varying concentrations of aerosols are depicted in Figure 14 from the model. The general shapes of the curves C and D are similar to the plots of A(N) derived from our measurements in Figures 12 and 13. However, it should be noted that the model calculated the optical thickness through one atmosphere whereas the observed data are from the geometry shown in Figure 5.

Radiance values calculated by the model are reproduced in Figure 15 for solar depression angles of 0 and 6 degrees and for varying elevation angles. Model B includes only ozone and model C incorporates a "standard" aerosol content also. Again, it should be noted that the model is for ground observations and thus includes a considerably different absorption path along the line-of-sight than is encountered in the airborne observations. Due to the differences in the geometry, the solar depression angles and elevation angles are not directly comparable in the two methods. Nevertheless, the observations clearly contain the absorption effects as calculated by the theoretical model and thus potentially provide a method of measurement.

The method, if developed, would have some unique and useful advantages. In particular, the measurements are made in the visible region of the spectrum where accurate absolute calibration is relatively simple as compared to those methods that utilize the ultraviolet region in which calibration is a major problem. A comparison of results from the different methods might substantially improve the precision of each. The advantages of the aircraft observations as compared to ground sites include, (1) independence of local weather, (2) reduction of effects of lower atmosphere aerosols, and (3) mobility to observe at varying latitudes, and for special conditions.

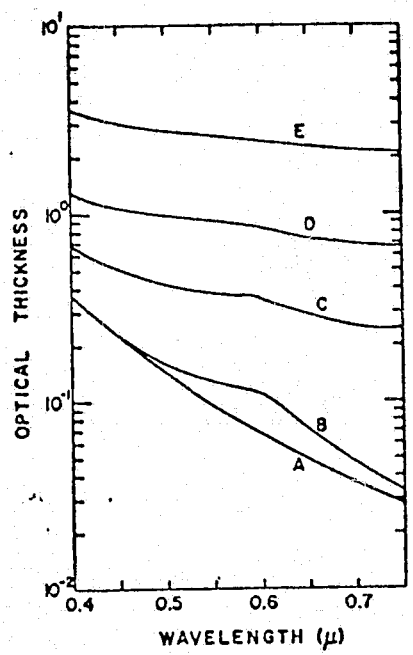


Figure 14. Model values of optical thickness (after Adams et al.)

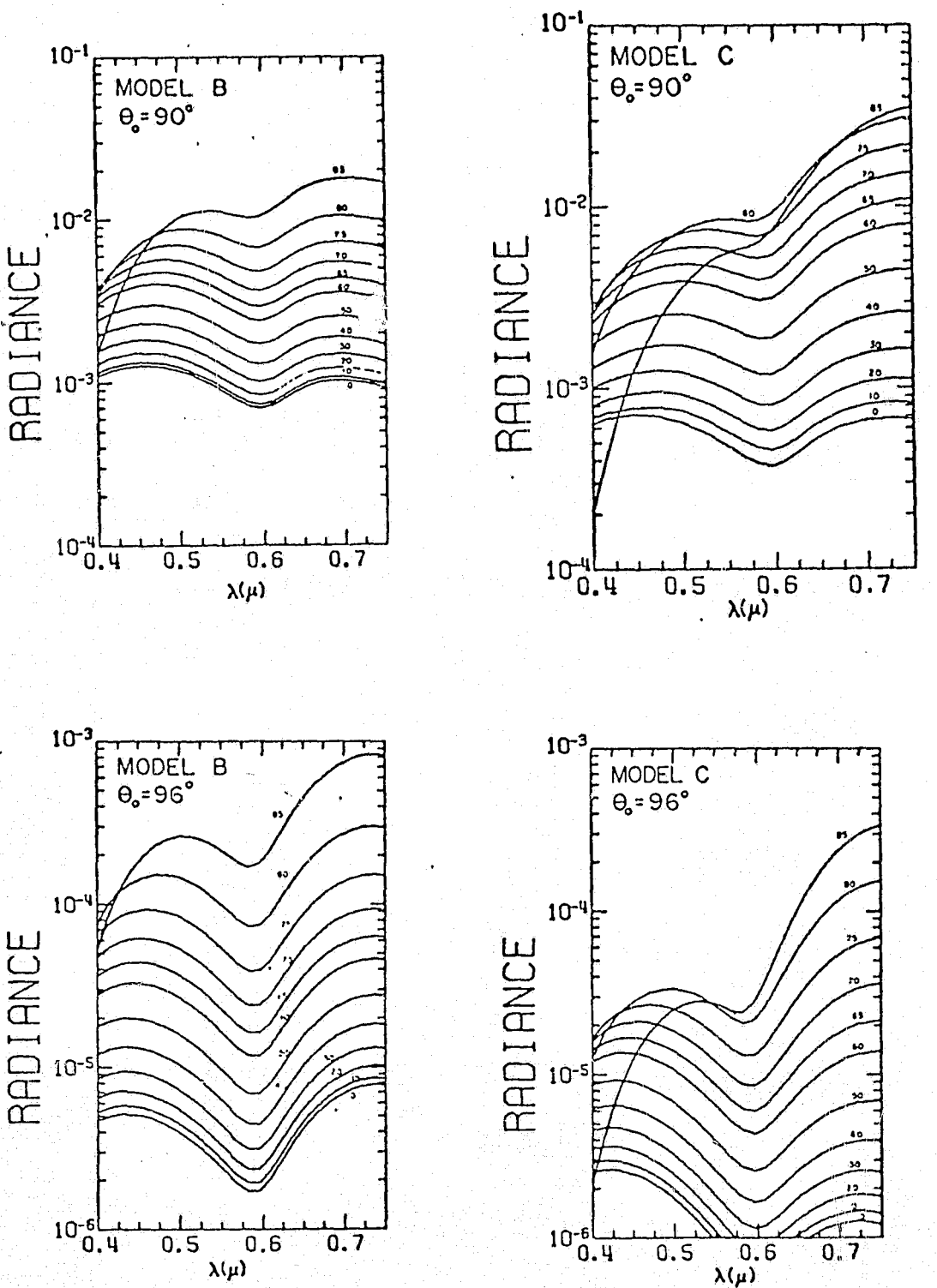


Figure 15. Radiance values from models (after Adams et al.)

The integrated effect which is observed in the twilight data complicates the interpretation but also smooths out local variations which occur in some other methods. The intergrated values are useful inputs to global models and for interpretation of similar observations from satellites.

Finally, the method may also be useful for the measurement of $NO_2$ which has absorption bands in the visible region. The aircraft method could be especially effective because $NO_2$ occurs at various levels in the atmosphere, but could be observed from different altitudes in order to establish the distribution.

In summary, the method appears to have useful application if the recording is photoelectric and a complete model is developed for the aircraft geometry.

## REFERENCES

Handbook of Geophysics and Space Environments, AFCRL, 1965.

Adams, C.M., G.M. Plass and G.W. Kattawar. J Atmosph Sci. 31: p. 1662-1674, 1974